

Online Video Streaming Super-Resolution with Adaptive Look-Up Table Fusion

Guanghao Yin, Xinyang Jiang, Shan Jiang, Zhenhua Han, Ningxin Zheng, Huan Yang, Donglin Bai, Haisheng Tan, Shouqian Sun, Yuqing Yang, Dongsheng Li, Lili Qiu

Abstract—This paper focuses on Super-resolution for online video streaming data. Applying existing super-resolution methods to video streaming data is non-trivial for two reasons. First, to support application with constant interactions, video streaming has a high requirement for latency that most existing methods are less applicable, especially on low-end devices. Second, existing video streaming protocols (*e.g.*, WebRTC) dynamically adapt the video quality to the network condition, thus video streaming in the wild varies greatly under different network bandwidths, which leads to diverse and dynamic degradations. To tackle the above two challenges, we proposed a novel video super-resolution method for online video streaming. First, we incorporate Look-Up Table (LUT) to lightweight convolution modules to achieve real-time latency. Second, for variant degradations, we propose a pixel-level LUT fusion strategy, where a set of LUT bases are built upon state-of-the-art SR networks pre-trained on different degraded data, and those LUT bases are combined with extracted weights from lightweight convolution modules to adaptively handle dynamic degradations. Extensive experiments are conducted on a newly proposed online video streaming dataset named LDV-WebRTC. All the results show that our method significantly outperforms existing LUT-based methods and offers competitive SR performance with faster speed compared to efficient CNN-based methods. Accelerated with our parallel LUT inference, our proposed method can even support online 720P video SR around 100 FPS.

Index Terms—Real-world Data, Online Video Streaming, Super resolution, Look-up Table.

I. INTRODUCTION

With the fast development of network infrastructure, video delivery techniques, and the growing demand of users, video streaming has become the “killer” application of the Internet in the past two decades [1]. Due to users’ steep expectations for quality, delivering high-definition (HD) video to end users is important. However, the quality of streamed video heavily depends on the network bandwidth between servers and clients. Streaming 4K videos require over 40 Mbps bandwidth per user [2], which is difficult to achieve in many areas. With the ever-increasing computational power of client devices and advances in deep learning, super-resolution (SR), which aims to restore high-resolution (HR) frames by adding the missing

details from low-resolution (LR) frames, has been considered as a promising direction to reduce the bandwidth requirement of streaming HD videos [2]–[9].

While previous works have achieved great progress [2], [5], [6], [8]–[11], existing super-resolution methods still face great challenges in real-world video streaming. First, it requires SR inference to be fast (*i.e.*, low-latency), especially for online scenarios like video conferences or cloud gaming. Second, existing video streaming protocols (*e.g.*, WebRTC [12]) heavily rely on bitrate adaptation to adaptively vary video compression degradations (*e.g.*, bitrate, quantization parameter, etc) according to network conditions, as shown in Fig. 1 and Fig. 4. Thus, SR models have to face spatially and temporally changing degradations, which challenge models’ capacity and adaptivity.

As a result, this paper focuses on developing a video super-resolution method specifically tackling the aforementioned two challenges in online video streaming. To meet the low-latency requirement, we propose to incorporate Look-Up Table (LUT) [13]–[19] into lightweight convolution modules, which replaces the time-consuming calculations with fast memory accesses. The great advantage of the look-up table is that it can store the mapping between low- and high-resolution frames for direct query, which significantly reduces the computation cost of neural networks. Furthermore, since existing LUT query and interpolation methods involve complicated control flow containing lots of if-else logical comparisons, its computation is unfriendly to accelerators, such as GPU, NPU, and FPGA [20]–[22]. Therefore, we also propose an efficient interpolation algorithm to accelerate LUT inference in parallel. Although possess great potential in low latency inference, existing LUT-based SR methods still face great challenge on spatial-temporal dynamic degradations, because these LUTs are usually transferred from simple-designed network structures with limited perception field [16]–[18]. Instead of using a single simple CNN, we build multiple look-up tables upon several existing state-of-the-art (SOTA) SR methods, which are pretrained with selected representative degradations. Then, the pixel-level LUT fusion is adaptively conducted based on larger frame patches to adapt to degradation variation.

As shown in Fig. 2, our Look-Up Table based video super-resolution method for Online Video Streaming (VS-LUT) consists of two parallel branches. On the spatial branch, we propose a pixel-level LUT fusion to adaptively handle dynamic degradations. A set of LUT bases are first converted from SOTA SR neural networks pre-trained on data with groups of static representative degradations, and then the converted LUT bases are fused by different linear combinations to handle

Guanghao Yin and Shouqian are with the Key Laboratory of Design Intelligence and Digital Creativity of Zhejiang Province, Zhejiang University, Hangzhou, China. Shan Jiang and Haisheng Tan are with University of Science and Technology of China, Hefei, China. Xinyang Jiang, Zhenhua Han, Ningxin Zheng, Huan Yang, Donglin Bai, Yuqing Yang, Dongsheng Li and Lili Qiu are with the Shanghai AI/ML Group, Microsoft Research Asia, Shanghai, China.

E-mail: {ygh_zju, ssq}@zju.edu.cn, {jiangshan, hstan}@ustc.edu.cn, {zhenhua.han, ningxin.zheng, huan.yang, donglinbai, yuqing.yang, dongsheng.li, liliqu, xinyangjiang}@microsoft.com

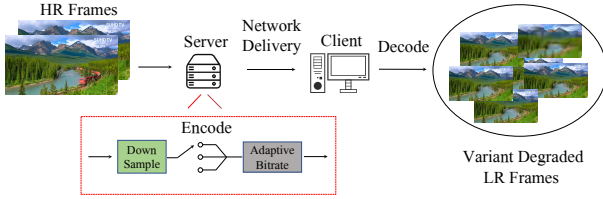


Fig. 1. Procedure of online video streaming. In online bitstreams, a server uses the Adaptive Bitrate (ABR) algorithm to encode frames at multiple bitrates for delivery, and then clients decode the received frames. During this adaptive delivery, the spatial-temporal dynamic degradations are inevitably introduced.

different degraded frame patches. On the temporal branch, a light-weight bias predictor is applied to further refine the spatial SR results with temporal information from history frames and motion vector priors.

To evaluate the performance of existing SR models under real-world scenario, we build a new real-world video streaming SR dataset named LDV-WebRTC, where Web Real-Time Communication (WebRTC) [12] is used to deliver the videos in LDV 2.0 dataset [23] with Adaptive Bitrate Streaming (ABR) algorithm under different network conditions. Extensive experiments reveal that our method can significantly outperform existing LUT-based models on both video quality and inference latency, and achieve comparable performance with efficient CNN-based SR models at a much faster speed.

In conclusion, our work contributes to threefold: (1) We present a novel LUT-based SR method specifically for Online Video Streaming (VS-LUT), which achieves real-time process latency and variant degradation adaptation by fusing various LUT bases built upon a pool of state-of-the-art SR models; (2) We collect a new real-world video streaming SR dataset (LDV-WebRTC), consisting of paired LR-HR frames and motion vector priors to facilitate the research of online video streaming SR; (3) With our lightweight modules and parallel LUT acceleration, our model achieves superior performance than existing LUT-based methods, and offers competitive video quality improvement with faster speed compared to efficient CNN-based SR methods.

II. RELATED WORK

A. Adaptive Online Bitstream

Adaptive online streaming aims to handle unpredictable bandwidth variations for high-quality video delivery. In online bitstreams, a server first encodes image frames at multiple bitrates for delivery, and then the client uses an ABR algorithm to select suitable video quality and decode the received frames [24]. During this adaptive delivery, coding artifacts are inevitably introduced [25]. The ABR algorithm controls Video Coding Protocols, such as H.264/AVC [26] or HEVC [27], to compress image frames with dynamic quantization parameters (QP) in both spatial and temporal dimensions. Therefore, one of the major challenges for high-quality online streamings is to handle the spatial-temporal dynamic degradations adaptively.

B. Super-Resolution

Super-resolution aims to restore HR images by adding the missing details from LR images. Since the pioneering

SRCNN [3], deep learning approaches [3], [4], [6], [7] have exhibited impressive performance in single-image SR (SISR) tasks. Considering the potential dependency in consecutive frames, various video SR (VSR) models [2], [5], [8], [9], [28], [29] with the optical flow alignment, deformable convolution or transformer have achieved great success to explore exploiting the temporal coherence among LR frames. However, many of them have a deep neural architecture, which brings heavy computing costs. Currently, there has been an increasing interest in fast SR and some great methods have been proposed. CARN [5] replaces the conventional convolutions with group convolutions, which reduce the parameters of its original big model. VESPCN [7] uses lightweight motion estimation and pixel-shuffle modules to conduct spatial-temporal upscaling. RRN [2] even removes the optical flow, but directly uses hidden states of recurrent proceedings to involve temporal information. However, they are still based on a certain amount of convolutional layers and thus have the potential to achieve faster speed.

C. Look-Up Table

Look-Up Table is an efficient tool for classic image processing because it can replace complex computations with retrieval operations. The pre-defined LUT has been widely used as the template to adjust the pixel distribution in photo editing and camera imaging [13]. Recent deep models have also extended LUTs to low-level vision tasks [13]–[17]. For color enhancement, Zeng *et al.* [13] first combine the learnable 3D LUT with convolutional modules to achieve LUT adaption at the image-level. Yang *et al.* [30] propose a more flexible sampling point allocation to adaptively learn the non-uniform sampling intervals in the 3D color space. Liu *et al.* [15] propose a learnable context-aware 4D LUT to achieve content-dependent enhancement. Recently, some new attempts have also been proposed for super-resolution. SR-LUT [16] first use a single 4D LUT to transfer the LR-HR mappings from a pretrained SR model with small receptive field (RF). And SPLUT [17] uses the parallel cascaded LUTs to process the high and low 4-bit components of 8-bit LR images. Meanwhile, the padding aggregations are also applied to enlarge the receptive field of LUT. Nevertheless, the fixed LUT mapping from the simple-designed network structures still limit their performance for dynamic degradations.

III. METHOD

A. Network Architecture

As shown in Fig. 2, we design the VSR network with adaptive LUT fusion for online video streaming, which contains two parallel branches. The spatial branch learns a linear combination of LUT bases built from pretrained SR networks to handle the dynamic degradation in the spatial dimension, and the temporal branch further refines the LUT outputs with temporal information from history frames and the priors of codec (i.e. motion vectors).

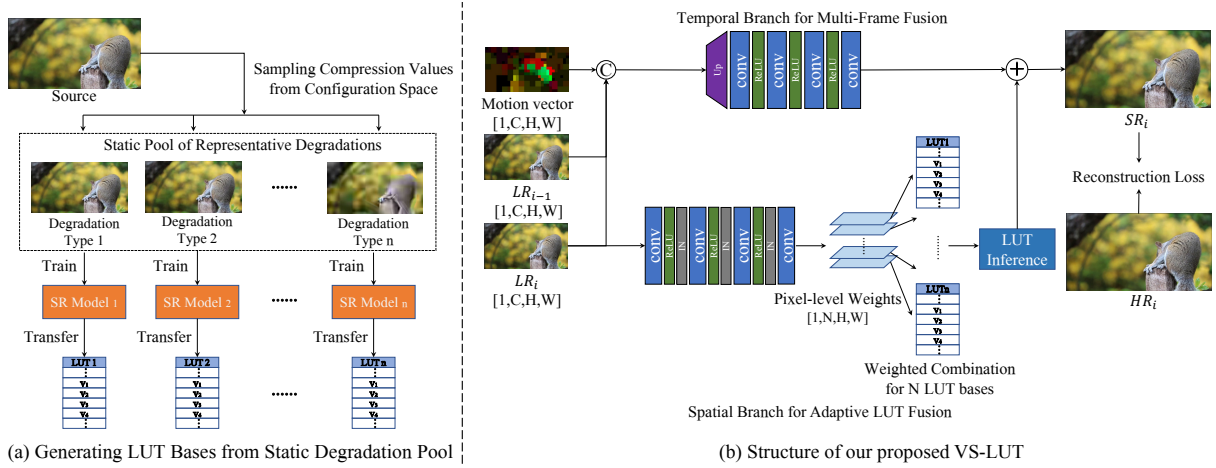


Fig. 2. The Overall scheme of our proposed VS-LUT. (a) First, a set of n LUT bases are built upon n SR networks pre-trained on n static representative degradations by sampling from the configuration space. (b) Then, the spatial and temporal branches of our VS-LUT conduct adaptive LUT fusion and multiple-frame fusion in parallel, and the outputs of the two branches are added to get the final SR results.

B. Spatial Branch for Adaptive LUT Fusion

As explained before, the challenge of online streaming SR is to handle the dynamic degradations in real-time speed and low latency. Although LUT achieves fast inference with small parameters by directly storing the input-output mapping of deep CNN models, existing LUT-based SR methods [16], [17] still cannot get promising results in the scenario of online streaming. First, their LUTs are transferred from the single SR model with a very simple network structure, which limits their ability to adapt to complicated degradation. Moreover, the inference of their LUTs for each pixel is only conducted inside the small query patch. Hence, their small receptive fields provide limited texture and structure information, which also creates a large gap for online streaming SR. As a result, we propose to build multiple LUT bases, each of which is transferred from a state-of-the-art SR network trained for specific static degradation, and during inference, LUT bases are adaptively fused for different frame patches with different degradations.

In this section, we elaborate on how to construct the LUT bases (3.2.1) and how to dynamically fuse the LUT bases to process each pixel (3.2.2). Moreover, we present an efficient LUT query and interpolation method that makes LUT more compatible with parallel acceleration (3.2.3).

1) *Transferring SR Networks to LUT Bases:* Here, we introduce how to build LUT bases from different SR networks. The degradation variation of video streaming systems is mainly caused by the configuration changing of video compression. The combination of different compression parameters results in a huge compression configuration space, and it is infeasible to exhaust all the options in it. As a result, we build a static pool of representative degradations by sampling compression parameter settings from the configuration space. SR networks are then trained on the videos corresponding to each of the degradation in this pool, getting SR models specialized in specific degradations.

As shown in Fig. 2(a), in our experiments, we focus on the quantization parameter (QP), which is one of the most im-

portant parameters to control video compression performance. The higher QP indicates the higher compression ratio and lower video quality. We uniformly sample N different QP values from $D_{qp} \in [0, m]$ corresponding to N different degradations $\{D_i\}_{i=0}^N$, and use them to generate N video SR training subsets $\{\mathcal{X}^{D_i}\}_{i=1}^N$. As a result, N SR models $\{f_{sr_i}\}_{i=1}^N$ are trained on those N subsets. It should be noted that the structure of the SISR model has no restrictions and any SOTA methods can be applied for training.

Then pre-trained SR networks are then transferred to LUT bases, which are later dynamically fused to a spatial-temporal variant LUT. As explained in previous LUT works [13], [15]–[17], each LUT stores all possible input values and the corresponding output values of an SR network. Following SR-LUT [16], we create the full permutation of 8-bit 2×2 patches, which are 256^4 patches in total ranging from $[0,0,0,0]$ to $[255,255,255,255]$. The SR model f_{sr_i} takes each 2×2 patch as input, and we store all high-resolution $r \times r$ output patches into the LUT, each of which up-samples the left-upper pixel of the low-resolution patch by scale factor r . Eventually, when all permutations of input patches are processed by SR model f_{sr_i} , we get the transferred LUT_i with the size of $[256, 256, 256, 256, r, r]$. Moreover, we follow SR-LUT [16] to compress LUT_i by uniformly sampling the original LUT with the interval size of 16, resulting in the compressed LUT_i with the size of $[17, 17, 17, 17, r, r]$.

2) *Adaptive LUT Fusion:* Leveraging the power of the mixture of experts [31]–[33], by adaptively fusing LUTs transferred from pre-trained SR models for each frame patch, we believe it is possible to obtain a LUT that adapts to any degradation. Given LUT bases transferred from the SR networks, we obtain a spatial and temporal variant look-up table by fusing these LUT bases with different important weights at each pixel position. Specifically, a lightweight predictor is proposed to output the LUT combination weights for each pixel based on the content of the input frame. The weight predictor, denoted as f_w , consists of 4 convolution layers with Instance Normalization [34] and LeakyReLU [35]

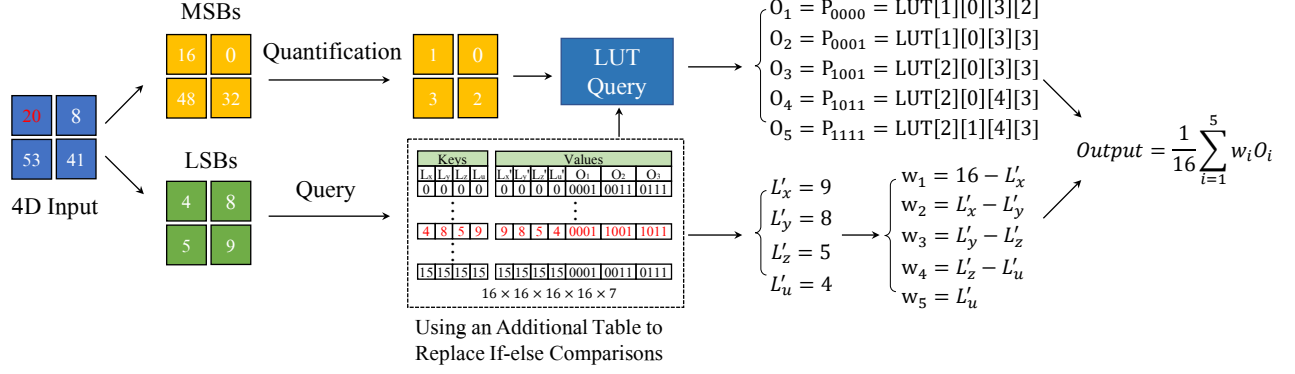


Fig. 3. An example of the implementation of our efficient LUT inference. Here, the quantization value is set as 16 to compress LUT.

TABLE I

THE NUMBER OF OPERATIONS OF DIFFERENT INTERPOLATIONS. DUE TO THE COMPLICATED IF-ELSE CONTROL FLOW, TETRAHEDRAL INTERPOLATION IS UNFRIENDLY TO ACCELERATORS LIKE BASIC CUDA OPERATORS. OUR INTERPOLATION NEEDS FEWER OPERATIONS AND CAN BE ACCELERATED BY CUDA.

Interpolation	Query	Multiplication	If-else Control Flow	Parallel Accelerator
Tetralinear	16	16	0	✓
Tetrahedral	5	5	24	✗
Ours	9	5	0	✓

operations. For the input LR frame $X \in \mathbb{R}^{h \times w \times 3}$, f_w outputs a weight tensor $W \in \mathbb{R}^{h \times w \times n}$, where n is the number of LUT bases. To obtain the SR result of a specific pixel in the frame $X_{i,j,k}$, the weighted LUT used for query is:

$$\hat{LUT}_{X_{i,j,k}} = W_{i,j,1} \times LUT_1 + \dots + W_{i,j,n} \times LUT_n. \quad (1)$$

It should be noted that the fusion operation is only conducted on the 4D lattice surrounding the input pixel, not the whole LUT. Moreover, since our weight predictor takes the entire frame as input, the weighted fusion is obtained based on a much larger receptive field, providing more spatial information than previous LUT-based methods [16], [17].

3) *Efficient LUT Interpolation*: Next, we introduce an efficient method to query the dynamically fused LUTs. Given the 4D input values, the output values of an anchor pixel $X_{i,j,k}$ are generated by querying and interpolating the nearest sampled points in LUT. Specifically, for the input (x, y, z, u) , we first conduct the look-up query operation to find its location in the 4D LUT lattice. As explained in previous LUT works [13], [15]–[17], the most significant bits (MSBs) of the input pixel value can be used for LUT location, and the least significant bits (LSBs) are used for interpolation. Hence, we separate the 8-bit input pixel values to high 4-bit integers (h_x, h_y, h_z, h_u) and low 4-bit decimals (l_x, l_y, l_z, l_u). Given the high 4-bit integers, we obtain the 4D LUT lattice surrounding the input pixel value, consisting of 16 adjacent sampling points $(h_x, h_x + 1, h_y, h_y + 1, h_z, h_z + 1, h_u, h_u + 1)$. The low 4-bit decimals (l_x, l_y, l_z, l_u) represent the distance between 4 input pixels (x, y, z, u) to their nearest points.

For interpolation, we choose the tetrahedral interpolation method [36], which needs only 5 multiplications with the values of 5 bounding vertices of 4-simplex geometry, much faster than tetralinear interpolation for 4D input. However, in practice, finding the 5 vertices among all total 24 neighboring vertices based on low 4-bit decimals (l_x, l_y, l_z, l_u) is implemented with 24 control flow instructions, which is unfriendly to parallel accelerators, resulting in a low inference speed. For example, CUDA operators do not support such flow control operation for parallel acceleration.

Here, we accelerate the tetrahedral interpolation by replacing the complicated control flow with the mapping table query. As shown in Table II, 24 logical statements in tetrahedral interpolation are equivalent to sorting the order of 4 input pixels from small to large. Therefore, we can use an additional table to store the sorted 4 values (x', y', z', u') and their 5 corresponding neighboring vertices (O_0, O_1, O_2, O_3, O_4) for all 256^4 4D permutations.

Since only the sorted LSBs determine the interpolation weights, the size of the mapping table can be efficiently compressed to $[16, 16, 16, 16, 7]$ by only storing 4-bit 4D-LSB permutations instead 256^4 8-bit 4D-pixel permutations. Moreover, the relative index of O_0 and O_4 are kept fixed at 0000 and 1111, and we only need to store the index of (O_1, O_2, O_3) . Once the order table is pre-defined, the comparison and flow control operation can be replaced by query, and the LUT inference can be accelerated in parallel.

Therefore, our accelerated LUT inference can be defined as three steps: (1) For the input (x, y, z, u) , we first separate the MSBs (h_x, h_y, h_z, h_u) and LSBs (l_x, l_y, l_z, l_u); (2) We query the pre-defined order table to get the sorted LSBs (l'_x, l'_y, l'_z, l'_u) and the binary index of (O_1, O_2, O_3) ; (3) we conduct the unified tetrahedral interpolation with the additional order table. As shown in Table I, the number of operations of our accelerated interpolation is smaller and can be easily deployed to accelerators. In our work, we use CUDA accelerator to conduct parallel computation.

Here, we present more details and implementation of our efficient LUT inference. As explained before, the commonly used tetrahedral interpolation involves 24 complicated control flows containing lots of if-else logical comparisons, which is unfriendly to accelerators, such as GPU, NPU,

TABLE II

THE 24 CONTROL FLOWS OF TETRAHEDRAL INTERPOLATION EQUIVALENT FOR 4D SPACE, ALSO PRESENTED IN SR-LUT [16]. SINCE THE CONTROL FLOWS ARE UNFRIENDLY FOR PARALLEL ACCELERATORS LIKE GPU, WE USE AN ADDITIONAL TABLE TO REPLACE THE IF-ELSE LOGICAL OPERATIONS AND UNIFORMLY CONDUCT THE INTERPOLATION.

Condition	w_1	w_2	w_3	w_4	w_5	O_2	O_3	O_4
$L_x > L_y > L_z > L_u$	$W - L_x$	$L_x - L_y$	$L_y - L_z$	$L_z - L_u$	L_u	P_{1000}	P_{1100}	P_{1110}
$L_x > L_y > L_u > L_z$	$W - L_x$	$L_x - L_y$	$L_y - L_u$	$L_u - L_z$	L_z	P_{1000}	P_{1100}	P_{1101}
$L_x > L_u > L_y > L_z$	$W - L_x$	$L_x - L_u$	$L_u - L_y$	$L_y - L_z$	L_z	P_{1000}	P_{1001}	P_{1101}
$L_u > L_x > L_y > L_z$	$W - L_u$	$L_u - L_x$	$L_x - L_y$	$L_y - L_z$	L_z	P_{0001}	P_{1001}	P_{1101}
$L_x > L_z > L_y > L_u$	$W - L_x$	$L_x - L_z$	$L_z - L_y$	$L_y - L_u$	L_u	P_{1000}	P_{1010}	P_{1110}
$L_x > L_z > L_u > L_y$	$W - L_x$	$L_x - L_z$	$L_z - L_u$	$L_u - L_y$	L_y	P_{1000}	P_{1010}	P_{1011}
$L_x > L_u > L_z > L_y$	$W - L_x$	$L_x - L_u$	$L_u - L_z$	$L_z - L_y$	L_y	P_{1000}	P_{1001}	P_{1011}
$L_u > L_x > L_z > L_y$	$W - L_u$	$L_u - L_x$	$L_x - L_z$	$L_z - L_y$	L_y	P_{0001}	P_{1001}	P_{1011}
$L_z > L_x > L_y > L_u$	$W - L_z$	$L_z - L_x$	$L_x - L_y$	$L_y - L_u$	L_u	P_{0010}	P_{1010}	P_{1110}
$L_z > L_x > L_u > L_y$	$W - L_z$	$L_z - L_x$	$L_x - L_u$	$L_u - L_y$	L_y	P_{0010}	P_{1010}	P_{1011}
$L_z > L_u > L_x > L_y$	$W - L_z$	$L_z - L_u$	$L_u - L_x$	$L_x - L_y$	L_y	P_{0010}	P_{0011}	P_{1011}
$L_u > L_z > L_x > L_y$	$W - L_u$	$L_u - L_z$	$L_z - L_x$	$L_x - L_y$	L_y	P_{0001}	P_{0011}	P_{1011}
$L_y > L_x > L_z > L_u$	$W - L_y$	$L_y - L_x$	$L_x - L_z$	$L_z - L_u$	L_u	P_{0100}	P_{1100}	P_{1110}
$L_y > L_x > L_u > L_z$	$W - L_y$	$L_y - L_x$	$L_x - L_u$	$L_u - L_z$	L_z	P_{0100}	P_{1100}	P_{1101}
$L_y > L_u > L_x > L_z$	$W - L_y$	$L_y - L_u$	$L_u - L_x$	$L_x - L_z$	L_z	P_{0100}	P_{0101}	P_{1101}
$L_u > L_y > L_x > L_z$	$W - L_u$	$L_u - L_y$	$L_y - L_x$	$L_x - L_z$	L_z	P_{0001}	P_{0101}	P_{1101}
$L_y > L_z > L_x > L_u$	$W - L_y$	$L_y - L_z$	$L_z - L_x$	$L_x - L_u$	L_u	P_{0100}	P_{0110}	P_{1110}
$L_y > L_z > L_u > L_x$	$W - L_y$	$L_y - L_z$	$L_z - L_u$	$L_u - L_x$	L_x	P_{0100}	P_{0110}	P_{0111}
$L_y > L_u > L_z > L_x$	$W - L_y$	$L_y - L_u$	$L_u - L_z$	$L_z - L_x$	L_x	P_{0100}	P_{0101}	P_{0111}
$L_u > L_y > L_z > L_x$	$W - L_u$	$L_u - L_y$	$L_y - L_z$	$L_z - L_x$	L_x	P_{0001}	P_{0101}	P_{0111}
$L_z > L_y > L_x > L_u$	$W - L_z$	$L_z - L_y$	$L_y - L_x$	$L_x - L_u$	L_u	P_{0010}	P_{0110}	P_{1110}
$L_z > L_y > L_u > L_x$	$W - L_z$	$L_z - L_y$	$L_y - L_u$	$L_u - L_x$	L_x	P_{0010}	P_{0110}	P_{0111}
$L_z > L_u > L_y > L_x$	$W - L_z$	$L_z - L_u$	$L_u - L_y$	$L_y - L_x$	L_x	P_{0010}	P_{0011}	P_{0111}
else	$W - L_u$	$L_u - L_z$	$L_z - L_y$	$L_y - L_x$	L_x	P_{0001}	P_{0011}	P_{0111}

and FPGA [20]–[22]. Therefore, we attempt to conduct an efficient strategy to accelerate LUT inference in parallel. As shown in Table II, the 24 logical statements (x, y, z, u) in tetrahedral interpolation are equivalent to sorting the order of 4 input pixels from small to large. Since all input permutations are countable, we can use an additional table to store the sorted 4 values (x', y', z', u') . The indexes of 5 corresponding neighboring vertices $(O_1, O_2, O_3, O_4, O_5)$ can also be store according to the 24 control flow instructions in Table II. It should be noted that the relative indexes of O_1 and O_5 are kept fixed at 0000 and 1111, and we only need to store the indexes of (O_2, O_3, O_4) . Moreover, only the least significant 4-bits determine the weights $(w_1, w_2, w_3, w_4, w_5)$, our additional table only needs to save 16^4 permutations.

An example of our efficient LUT inference is presented in Fig. 3. For the input (x, y, z, u) , we first separate the most significant bits (MSBs) (H_x, H_y, H_z, H_u) and the least significant bit (LSBs) (L_x, L_y, L_z, L_u) . The MSBs of the input pixel value can be used for LUT location and least significant bits (LSBs) are used for interpolation. Specifically, we separate the 8bit input pixel values to high 4bit integers (H_x, H_y, H_z, H_u) as:

$$H_x = \left\lfloor \frac{x}{16} \right\rfloor, H_y = \left\lfloor \frac{y}{16} \right\rfloor, H_z = \left\lfloor \frac{z}{16} \right\rfloor, H_u = \left\lfloor \frac{u}{16} \right\rfloor, \quad (2)$$

and low 4bit decimals (L_x, L_y, L_z, L_u) as:

$$\begin{aligned} L_x &= x - H_x \times W, L_y = y - H_y \times W, \\ L_z &= z - H_z \times W, L_u = u - H_u \times W, \end{aligned} \quad (3)$$

where $\lfloor \cdot \rfloor$ is the floor function, and W represents the quantization value to compress the LUT, which is set as 16 in our paper. Then, we query the pre-defined additional table to get

the sorted LSBs (L'_x, L'_y, L'_z, L'_u) and the binary indexes of (O_2, O_3, O_4) . When we get the sorted LSBs (L'_x, L'_y, L'_z, L'_u) , the calculation of interpolation weights $(w_1, w_2, w_3, w_4, w_5)$ doesn't need the if-esle judgement in Table II, but can be uniformly defined as:

$$\begin{aligned} w_1 &= W - L'_x, w_2 = L'_x - L'_y, w_3 = L'_y - L'_z, \\ w_4 &= L'_z - L'_u, w_5 = L'_u. \end{aligned} \quad (4)$$

When we get the binary indexes of (O_2, O_3, O_4) , the values of $(O_1, O_2, O_3, O_4, O_5)$ can be accessed by using their binary indexes and MSBs (H_x, H_y, H_z, H_u) to conduct LUT query. For example, if the index of O_2 is 0001, the value of O_2 is $P_{0001} = LUT[H_x][H_y][H_z][H_u + 1]$. Finally, the output of weighted interpolation are calculated as:

$$Output = \frac{1}{W} \sum_{i=1}^5 w_i * O_i. \quad (5)$$

During the LUT interpolation, the weighted combination of N LUT bases can also be conducted in parallel.

C. Temporal Branch for Multi-Frame Processing

Like most of the VSR methods, to fully utilize the temporal information, our proposed model contains a temporal branch responsible for refining the result of the LUT branch with history frames and object motions. To achieve fast speed and low latency for online streaming, the commonly used modules, such as optical flow alignment, deformable convolution and transformer [2], [5], [8], [9], are not suitable for our task. Moreover, the future frames cannot be utilized when the current frame is processed in the online scenario.

As shown in Fig. 2(b), our temporal branch only uses of 4 conventional layers with LeakyReLU [35] to fuse the previous and current frames. To get more motion-related information, the temporal branch also leverages an easily accessed video streaming prior, which are the motion vectors already extracted by the video codec of the streaming system. Similar to optical flow, it is a coarse approximation of the patch-level correspondence and alignment between two frames. But unlike optical flow, it's the prior knowledge of the streaming system, which can be directly obtained with no extra calculation. To avoid additional computation cost, we add the motion vector between two frames as the additional feature map for better temporal fusion.

IV. NEW DATASET FOR ONLINE STREAMING VSR

Since existing datasets either use raw video frames [23], [37], [38] or compressed with fixed presets [23], they do not reflect the diverse and time-varying degradation of online video streaming. Hence, we collect a new video SR dataset to address real-world challenges with more realistic online video streaming settings, named LDV-WebRTC.

WebRTC [12] is a real-time communication protocol that is widely used to stream real-time videos to browsers or mobile devices. We build a video streaming prototype based on WebRTC, which uses a server to stream low-resolution videos to a laptop client via a router. The router uses Linux

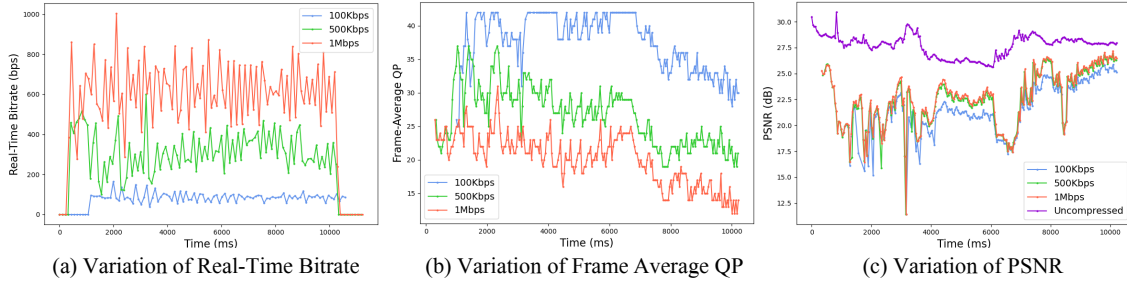


Fig. 4. The variations of real-time bitrates, frame-average QP, and PSNR of streamed test video 005 using our WebRTC testbed under 100Kbps, 500Kbps and 1Mbps bandwidths. When the bandwidth decreases from 1Mbps to 100Kbps, the QP value increases, which causes lower image quality. Therefore, online streaming degradation is much more challenging.

to control the network bandwidth between the server and the client to emulate the diverse bandwidth settings of real-world applications. We collect all 335 high-resolution videos in the LDV 2.0 dataset [23], containing a rich diversity of content scenes whose frame resolution is 960×512 . The high-resolution frames are downsampled by $4\times$ in bicubic mode to get 240×128 low-resolution frames, which are encoded via FFmpeg-H.264 [39] and then transmitted by the servers. The WebRTC server enables Adaptive Bitrate streaming (ABR) that adjusts encoding quality with QP values in a range of $[0, 50]$, according to factors including network bandwidth, encoding latency, and decoding latency. A larger QP leads to worse quality of encoded frames. After receiving an encoding video stream, the client decodes it into a sequence of decoded low-resolution frames with timestamps. The target of video streaming SR is to restore those received LR frames. To involve different network conditions, three representative types of networks are emulated in the router with an average bandwidth of 100kbps, 500kbps, and 1Mbps. Note that, when bandwidth is limited, not all frames are successfully received due to frame drop. Thus we align the decoded frames at the client with the original high-resolution frames using encoding timestamps. In addition to the decoded frames, we also collect the motion vector priors extracted by the video codec of the streaming system.

Fig. 4 illustrates the statistic example of real-time bitrates, QP and PSNR of streamed frames using our WebRTC testbed under different network bandwidths. It's clear that the PSNR of real streamed video fluctuated more severely due to the real-time encoding-decoding pipeline and the bitrates variation. The QP values of encoded frames also vary greatly and sometimes even trigger resolution changes (*i.e.* WebRTC's default strategy degrades resolution when the frame-average QP is quite large). Moreover, the frame drop also happens frequently for online streaming. All those observations prove the necessity of building a more realistic dataset that reflects the diverse and time-varying degradation of real-world online video streaming. In conclusion, our dataset consists of the aligned LR frames of the client, their original HR versions of the server, and the bitstream priors under 100kbps, 500kbps, and 1Mbps bandwidths.

Here, we present more statistical results about our real-collected LDV-WebRTC dataset. Table III illustrates the statistical results of average real-time bitrates, QP and PSNR

TABLE III
STATISTICAL RESULTS OF OUR LDV-WEBRTC DATASET.

Bandwidth	Dataset	Bitrate (Kbps)	QP	PSNR (dB)	Frame Number
100Kbps	Training	85.15	30.79	24.37	63792
	Validation	84.79	29.75	23.72	4415
	Test	82.26	29.87	23.31	5558
500Kbps	Training	334.56	20.90	25.04	74207
	Validation	340.05	18.80	24.68	5926
	Test	322.05	20.42	24.27	5980
1Mbps	Training	497.22	17.73	25.21	73603
	Validation	476.10	16.21	24.79	5939
	Test	486.48	17.54	24.35	6078

of streamed frames on the training, validation, and test sets, which are collected by our WebRTC testbed under different network bandwidths. When the bandwidth setting decreases from 1Mbps to 100Kbps, the real bitrate decreases and the online streaming system uses lower QP to compress frames, which causes lower image quality. Moreover, the frame drop also happens more frequently when the bandwidth decreases. All those observations reveal the online streaming degradations are dynamic and challenging.

V. EXPERIMENTS

A. Experimental Setting

Datasets. Since we focus on the real scenario of online streaming, the experiments are conducted on the proposed LDV-WebRTC dataset. We focus on the scale factor $r = 4$. To assess the model ability to deal with degradations under different bandwidths, we only use the LR-HR pairs under 1Mbps for training, and evaluate SR models on 100Kbps, 500Kbps, and 1Mbps testsets respectively. We also conduct more experiments on compression SR datasets, which can be found in Table V.

Evaluation Metrics. We evaluate the SR performance for online streaming from three perspectives: the number of model parameters, runtime, and the distortion quality of the generated results. Specifically, Peak Signal-to-Noise Ratio (PSNR) and Structural Similarity Index (SSIM) [26] are adopted for evaluation. To compare the running speed, we measure and report the runtime of super-resolving 320×180 LR images on one NVIDIA RTX 2080Ti GPU.

Implementation Details. As explained in Sec. III-B1, we uniformly select 6 QP values ($QP = 0, 10, 20, 30, 40, 50$)

TABLE IV

$\times 4$ SR MODEL COMPARISONS ON OUR REAL LDV-WEBRTC TESTSETS UNDER 100Kbps, 500Kbps, AND 1Mbps. THE LATENCY LEVELS REQUIRED BY DIFFERENT METHODS ARE SORTED FROM HIGH TO LOW. SIZE DENOTES THE STORAGE SPACE OR THE PARAMETER NUMBER OF EACH MODEL. THE ROW HIGHLIGHTED IN GRAY MEANS THE SR METHOD HAS UNBEARABLE HIGH LATENCY, AND THUS CANNOT BE APPLIED FOR ONLINE STREAMING. FOR ONLINE PRACTICAL SR METHODS, BEST AND SECOND BEST RESULTS ARE HIGHLIGHTED IN RED AND BLUE. RUNTIME IS MEASURED WITH 2080Ti GPU FOR GENERATING 1280×720 RESULTS. *: THE LUT-BASED METHODS ARE ACCELERATED BY OUR INTERPOLATION. †: THE STORAGE SPACE OF THE LUT-BASED METHOD.

Latency Level	Model	100Kbps PSNR / SSIM	500Kbps PSNR / SSIM	1Mbps PSNR / SSIM	Size	Runtime	FPS	Video (30FPS)	Gaming (60FPS)
High	BasicVSR++ [9]	23.95 / 0.6210	24.70 / 0.6754	25.11 / 0.6997	9.54M	418.5ms	2.34		
	TTVSR [8]	23.87 / 0.6246	24.73 / 0.6742	25.24 / 0.7012	6.72M	244.3ms	4.09		
	RCAN [6]	23.80 / 0.6165	24.64 / 0.6729	24.85 / 0.6960	15.6M	205.4ms	4.89	✗	✗
	SRResNet [4]	23.76 / 0.6141	24.53 / 0.6663	24.62 / 0.6878	1.52M	75.80ms	13.19		
Middle	RRN [2]	23.48 / 0.6121	24.48 / 0.6521	24.84 / 0.6811	3.36M	27.00ms	37.03		
	CARN [5]	23.77 / 0.6137	24.50 / 0.6565	24.74 / 0.6927	1.59M	25.30ms	39.53	✓	✗
	VESPCN [7]	23.25 / 0.6063	24.34 / 0.6427	24.50 / 0.6774	0.88M	22.84ms	43.78		
	SPLUT* [17]	23.34 / 0.6097	24.41 / 0.6333	24.55 / 0.6764	18.12MB†	21.81ms	45.85		
Low	BI	23.31 / 0.6031	24.27 / 0.6274	24.35 / 0.6724	-	-	-		
	PAN [40]	23.55 / 0.6123	24.50 / 0.6332	24.66 / 0.6742	0.27M	16.12ms	62.50		
	SR-LUT* [16]	23.45 / 0.5901	24.32 / 0.6198	24.42 / 0.6451	1.27MB†	11.60ms	79.37	✓	✓
	VS-LUT-CARN*	23.73 / 0.6123	24.46 / 0.6540	24.80 / 0.6803					
	VS-LUT-SRResNet*	23.78 / 0.6140	24.54 / 0.6558	24.87 / 0.6822	8.65MB†	10.23ms	97.75		
	VS-LUT-RCAN*	23.82 / 0.6163	24.52 / 0.6576	24.82 / 0.6816					

and use these QP values to encode 6 degraded video subsets $\{D_1, \dots, D_6\}$. Three state-of-the-art SR models, SRResNet [4], CARN [5], and RCAN [6] are trained on the 6 datasets and transferred to 3 groups of LUT bases. Finally, we train our network with 3 groups of LUT bases on 1Mbps data. Three trained models are denoted as VS-LUT-SRResNet, VS-LUT-CARN, and VS-LUT-RCAN.

The number of channels of spatial and temporal branches is set to 64. The number of output channels of pixel-level weight predictor is set to 6, matching the number of LUT bases. In training configurations, the image patch is randomly cropped with the size of 48×48 , and the batch size is set to 16. The whole VS-LUT is jointly trained by imposing Charbonnier loss on the final SR outputs. We use Adam optimizer with $\beta_1 = 0.9$ and $\beta_2 = 0.999$ to update model parameters. The initial learning rate is 10^{-4} . We conducted the model training with NVIDIA Tesla V100 GPUs.

B. Experiments on LDV-WebRTC Dataset

We compare our method with various SOTAs. Among these methods, SRResNet [4], CARN [5], and RCAN [6] are the base networks for LUT base construction. PAN [40] is a widely used single-image SR structure with low model complexity and fast inference speed. We also compare with two fast VSR methods VESPCN [7] and RRN [2]. Due to low latency requirement in online streaming scenario, it is infeasible to cache future frames for VSR models. As a result, we modify VESPCN by removing the next frame branch and only extract the spatial-temporal information with the previous and current frames. BasicVSR++ [9] and TTVSR [8] are much larger bi-directional VSR models. Although they are not appropriate for online scenarios, we still involve them as the performance upper bound. Moreover, we further compare two LUT-based SISR models, SR-LUT [16] and SPLUT [17]. Note that the GPU inference speed of the current SR-LUT

implementation is quite slow due to the large portion of if-else control flow operations and serial for-loop processing for each pixel. For a fair comparison, we also accelerate those LUT-based models with our efficient interpolation method in parallel, as explained in Sec. III-B3. We used the open-source codes provided by the authors to implement the compared methods. All methods use the same train-test set partition, where the training data with 1Mbps bandwidth are used, and the evaluations are conducted on 100Kbps, 500Kbps, and 1Mbps testsets.

All the evaluation results are reported in Table IV. Since the latency is quite important for online streaming, we further measure runtime and FPS to evaluate the model efficiency. Based on FPS, We categorize the compared SR methods into three types. We categorize methods with FPS lower than 30 as High Latency methods, which are hard to support online streaming applications. Low Latency group refers to methods with FPS higher than 60, fast enough to support high-frame-rate gaming. The rest methods in the range of 30 FPS and 60 FPS are marked as Middle Latency. Benefited from spatial-temporal feature extraction and deep network structure, VSR methods BasicVSR++ [9] and TTVSR [8], as well as SISR models RCAN [6] and SRResNet [4] achieve high PSNR/SSIM performance, in exchange of very high latency impractical to online streaming, due to their large neural network size. Compared with methods in the Middle Latency group, our model outperforms them with a marginal improvement in terms of PSNR and SSIM, and in the meantime achieves a much better latency and FPS. In low latency scenarios, our method can significantly outperform other lightweight models such as PAN [40] and LUT-based SR-LUT [16] in terms of PSNR/SSIM values and meanwhile achieves the lowest latency. The comparisons between our models using 3 types of LUT bases can also give some interesting findings. When the quality of LR frames decreases (*i.e.* 100Kbps), the LUT bases transferred from better SR structures (*i.e.* RCAN)

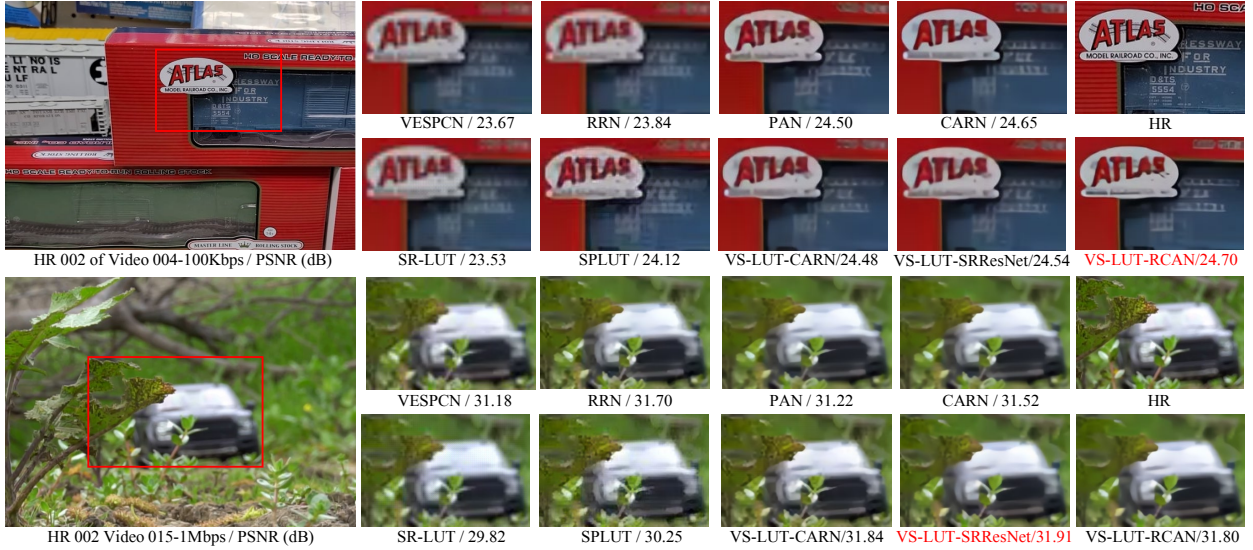


Fig. 5. SR perceptual results ($\times 4$) of images selected from 100Kbps and 1Mbps testsets. Best results are highlighted in red.

produce better results. Moreover, by comparing model sizes, we can see that our method only brings a linear increase in storage costs because of multiple LUT bases. We believe the model size of our VS-LUT is acceptable for current devices. All those results verify the effectiveness of our VS-LUT in the online streaming scenario.

Visual comparisons are shown in Fig. 6. Here, we choose practical SR methods in the Middle and Low Latency groups for comparisons. It can be seen that previous LUT-based methods, including SR-LUT [16] and SPLUT [17], fail to present natural details and produce more artifacts. Limited by less conventional layers and network parameters, the lightweight CNN-based SR models, such as PAN [40] and VESPCN [7], generate results with less high-frequency details. And our models produce less artifacts than previous LUT-based methods and present a similar level of sharpness to CARN [5] and RRN [2] at faster speed. In Fig. 6, we present more visual results of several representative efficient SR models on our LDV-WebRTC dataset.

C. Experiments on Static Compression Degradation

The LUT bases of our method are determined by the structure of SISR model and the corresponding training degradations of those SR models. In Manuscript, we have fused the LUT bases transferred from the same SR structure but trained with different training degradations to handle the dynamic online streaming degradations. Here, we further evaluate the effectiveness of the fusion with different SR structures, which are trained with the same static degradation. Specifically, we follow the NTIRE2022 challenge [23] to conduct experiments on the static $QP = 37$ compression degradation. Three SISR model SRResNet [4], CARN [5], and RCAN [6] are used as the base networks for LUT construction, and our model is denoted as VS-LUT-RCAN+SRResNet+CARN. All those 3 SR networks are trained with the same training set and three corresponding transferred LUTs are grouped as the bases for

TABLE V
 $\times 4$ SR MODEL COMPARISONS OF NTIRE2022 CHALLENGE TRACK3 ON SUPER-RESOLUTION AND QUALITY ENHANCEMENT OF COMPRESSED VIDEO. THE RESULTS FROM THE 1ST ROW TO 3RD ROW ARE DIRECTLY EXTRACTED FROM NTIRE2022 REPORT [23]. *: THE LUT-BASED METHODS ARE ACCELERATED BY OUR INTERPOLATION.

Model	PSNR	Runtime	Hardware
GY-Lab (BasicVSR++ [9] based) 1st [23]	24.23	11.5s	V100
AVRT (VSRTransformer [41] based) 9th [23]	23.52	2s	A100
Modern_SR (EDVR [42] based) 12th [23]	23.03	860ms	3080
RCAN [6]	22.96	205.4ms	2080ti
SRResNet [4]	22.93	75.80ms	2080ti
CARN [5]	22.89	25.30ms	2080ti
SP-LUT* [17]	22.87	21.81ms	2080ti
SR-LUT* [16]	22.61	11.60ms	2080ti
VS-LUT-RCAN+SRResNet+CARN*	23.32	10.23ms	2080ti

LUT fusion. And we follow the NTIRE2022 challenge [23] to train and test SR models on LDV 2.0 dataset.

The SOTA comparisons are presented in Table V. Except the SR models presented in Manuscript, we further add 3 novel methods presented in NTIRE2022 Report [23]. Although cannot outperform the deep VSR methods, such as the 1st winner model GY-Lab, our model still outperforms both LUT-based models and three SR base networks. Those results proves that the combination of LUT bases can also efficiently fuse the capabilities of different SR structures. In practice, the LUT fusion can be considered in both the training degradation and the SR structure.

D. Ablation Analysis

Effectiveness of Different Modules. Table VI shows the effectiveness of different modules in VS-LUT. When only one single-LUT base is applied, the basic model (A) is quite similar to SR-LUT [16], and it produces poor PSNR result, which proves the small receptive field and single-base neural networks cannot handle the dynamic degradations of online

TABLE VI

ABLATION STUDIES OF THE COMPONENTS. THE LUT BASES ARE TRANSFERRED FROM RCAN [6]. ALL THE RESULTS ARE EVALUATED ON 1MBPS TESTSET. EACH COMPONENT BRINGS IMPROVEMENTS IN PSNR.

	(A)	(B)	(C)	Our
Single-LUT Base	✓			
Multi-LUTs Adaptive Fusion		✓	✓	✓
Previous Frame Information			✓	✓
Motion Vector information				✓
Size (MB)	1.27	8.52	8.64	8.65
Runtime (ms)	2.84	4.07	10.21	10.23
PSNR (dB)	24.21	24.47	24.80	24.84

streaming. By adding adaptive LUT fusion, the PSNR has significantly increased by 0.26dB, showing that the pixel-level weight predictor can fuse the LUT bases from different static degradation pools to adaptively handle dynamic degradations. Since the weight predictor consists of 4 convolution layers, it cost more storage and computation, but the 8.52MB increase is acceptable for current devices. After adding temporal information from previous frames and the motion vector priors, the performances of our model are further improved, at the cost of lower inference speed. The commonly used temporal fusion modules like optical flow estimation or deformable convolution is too slow to be applied to online streaming, and hence we adopt a lightweight structure to process the easily available prior information. We believe that other novel and lightweight VSR modules can also be applied and further improve the performance of our framework.

Configurations of LUT Bases. First, the LUT bases of VS-LUT can be constructed from different SR networks. The last 3 rows of Table IV show how LUT bases transferred from different SR networks affect the performance of VS-LUT, where better performed SISR network can help the corresponding LUT bases to get better results in severe degradation. We also analyze how the number of LUT bases affects the performance of VS-LUT, where we evenly selected N QP values from the range of 0 to 50 where the corresponding videos are used to construct N LUT bases. As shown in Table VII, increasing the number of LUT bases constantly improves the SR performance. It reveals that more refined subsets generation can produce more fine-grained LUT bases, thus the pixel-level adaptive fusion can better handle severe dynamic degradations. However, more LUT bases brings more storage and computational cost. When the number of LUT bases is larger than 6, our model only has a minor improvement, and 6 LUT bases achieve the best trade-off between SR performance and model efficiency. In Table V, we also prove that the fusion of LUT bases from different SR structures is effective. In practice, the configuration of LUT bases, such as the number, the training degradation, and its correspondence SR structure can be determined by the scenario for the flexible model design.

LUT Sampling. For LUT-based SR methods [16], [17], the original LUT is commonly sampled with a quantization value to compress the size of LUTs. For our method, we also uniformly sample the LUT. In table VIII, we present the

TABLE VII

COMPARISON OF OUR MODEL WITH LUT BASES FROM DIFFERENT STATIC DEGRADATIONS. THE LUT NUMBER IS EQUAL TO THE NUMBER OF DEGRADED SUBSETS. WE CHOOSE THE NUMBER OF LUT BASES AS 6, CONSIDERING ACCURACY AND EFFICIENCY.

LUT Number	Storage	Runtime	1Mbps PSNR / SSIM
1	2.32 MB	8.64 ms	24.21 / 0.6231
3	4.84 MB	9.31 ms	24.60 / 0.6694
6	8.65 MB	10.23 ms	24.84 / 0.6816
12	16.27 MB	12.05 ms	24.89 / 0.6813

TABLE VIII

COMPARISON OF OUR VS-LUT-RCAN WITH DIFFERENT SAMPLING INTERVAL SIZES. WE SET THE SAMPLING INTERVAL SIZE AS 16 FOR OUR MODEL TO REDUCE THE LUT SIZE, MINIMIZING THE DROP OF THE ORIGINAL PERFORMANCE.

Sampling	LUT Storage	1Mbps PSNR / SSIM
2^0 (Full LUT)	384 GB	24.91 / 0.6875
2^2	1632 MB	24.90 / 0.6871
2^3	108 MB	24.87 / 0.6843
2^4 (Our)	7.644 MB	24.84 / 0.6816
2^5	612 KB	24.61 / 0.6740
2^6	59.35 KB	24.34 / 0.6538
2^8	2.304 KB	23.15 / 0.6459

comparisons of our VS-LUT models with different quantization values. The uncompressed LUT bases (2^0) produces the best results but have unbearable storage (384GB). When the sampling size decreases from 2^2 to 2^4 , the size of LUT significantly decreases from 1632MB to 7.644 MB while getting acceptable performance drop. Therefore, we choose the quantization value 16 as our default setting. If the LUT size matters, sampling sizes 2^5 and 2^6 could also be considered. For practical implementation, the sampling size should be considered as the tradeoff between the storage cost and the performance.

Effectiveness of Interpolation Acceleration. Table IX verifies the effectiveness of our proposed efficient LUT query and interpolation method. As shown in Table IX, by adopting an additional mapping table to replace the if-else control flow operations, both SR-LUT [16] and our VS-LUT achieves more than 35 times inference acceleration on GPU devices. It proves our interpolation can help further LUT-based methods for faster speed with parallel accelerators.

VI. CONCLUSION

In this paper, we propose a novel video super-resolution method for online streaming with adaptive LUT fusion, called VS-LUT. To achieve low process latency and adapt to time-varying degradations in video streaming, we proposed to dynamically fuse a set of LUT bases transferred from different SOTA SR networks trained on a selected pool of static degradations. The temporal information from previous frames and the motion vector priors are also considered in VS-LUT. Moreover, we conduct an efficient interpolation method to efficiently accelerate the LUT inference in parallel. A new real-world streaming dataset LDV-WebRTC is proposed for

TABLE IX

RUNTIME OF LUT INTERPOLATION INFERENCE. AFTER USING OUR ACCELERATED TETRAHEDRAL INTERPOLATION, THE PARALLEL ACCELERATION CAN BE APPLIED WITHOUT IF-ELSE CONTROL FLOW INSTRUCTIONS. THE INFERENCE SPEEDS OF BOTH OUR MODEL AND SR-LUT GET SIGNIFICANTLY IMPROVED.

Model	Our Acceleration	If-else Control Flow	Runtime
SR-LUT [16]	\times	\checkmark	381.89 ms
	\checkmark	\times	11.60 ms
Our VS-LUT	\times	\checkmark	516.21 ms
	\checkmark	\times	10.23 ms

performance evaluation in online video streaming scenario. Comprehensive experiments demonstrate the effectiveness, efficiency, and flexibility of the proposed method. Although how to enlarge receptive fields of LUTs and apply them to video tasks are still open issues, we believe the LUT-based SR model has great potential for realistic scenarios.

REFERENCES

- [1] Z. Lu, H. Xia, S. Heo, and D. Wigdor, "You watch, you give, and you engage: a study of live streaming practices in china," in *Proceedings of the 2018 CHI conference on human factors in computing systems*, 2018, pp. 1–13. **1**
- [2] T. Isobe, F. Zhu, X. Jia, and S. Wang, "Revisiting temporal modeling for video super-resolution," *BMVC*, 2020. **1, 2, 5, 7, 8, 12**
- [3] C. Dong, C. C. Loy, K. He, and X. Tang, "Image super-resolution using deep convolutional networks," *IEEE transactions on pattern analysis and machine intelligence*, vol. 38, no. 2, pp. 295–307, 2015. **1, 2**
- [4] C. Ledig, L. Theis, F. Huszár, J. Caballero, A. Cunningham, A. Acosta, A. Aitken, A. Tejani, J. Totz, Z. Wang *et al.*, "Photo-realistic single image super-resolution using a generative adversarial network," in *Proceedings of the IEEE conference on computer vision and pattern recognition*, 2017, pp. 4681–4690. **1, 2, 7, 8**
- [5] N. Ahn, B. Kang, and K.-A. Sohn, "Fast, accurate, and lightweight super-resolution with cascading residual network," in *Proceedings of the European conference on computer vision (ECCV)*, 2018, pp. 252–268. **1, 2, 5, 7, 8, 12**
- [6] Y. Zhang, K. Li, K. Li, L. Wang, B. Zhong, and Y. Fu, "Image super-resolution using very deep residual channel attention networks," in *Proceedings of the European conference on computer vision (ECCV)*, 2018, pp. 286–301. **1, 2, 7, 8, 9**
- [7] J. Caballero, C. Ledig, A. Aitken, A. Acosta, J. Totz, Z. Wang, and W. Shi, "Real-time video super-resolution with spatio-temporal networks and motion compensation," in *Proceedings of the IEEE conference on computer vision and pattern recognition*, 2017, pp. 4778–4787. **1, 2, 7, 8**
- [8] C. Liu, H. Yang, J. Fu, and X. Qian, "Learning trajectory-aware transformer for video super-resolution," in *Proceedings of the IEEE/CVF Conference on Computer Vision and Pattern Recognition*, 2022, pp. 5687–5696. **1, 2, 5, 7**
- [9] K. C. Chan, S. Zhou, X. Xu, and C. C. Loy, "BasicVSR++: Improving video super-resolution with enhanced propagation and alignment," in *Proceedings of the IEEE/CVF Conference on Computer Vision and Pattern Recognition*, 2022, pp. 5972–5981. **1, 2, 5, 7, 8**
- [10] F. Yang, H. Yang, J. Fu, H. Lu, and B. Guo, "Learning texture transformer network for image super-resolution," in *Proceedings of the IEEE/CVF conference on computer vision and pattern recognition*, 2020, pp. 5791–5800. **1**
- [11] Z. Qiu, H. Yang, J. Fu, and D. Fu, "Learning spatiotemporal frequency-transformer for compressed video super-resolution," in *Proceedings of the European conference on computer vision (ECCV)*, 2022. **1**
- [12] A. B. Johnston and D. C. Burnett, *WebRTC: APIs and RTCWEB protocols of the HTML5 real-time web*. Digital Codex LLC, 2012. **1, 2, 5**
- [13] H. Zeng, J. Cai, L. Li, Z. Cao, and L. Zhang, "Learning image-adaptive 3d lookup tables for high performance photo enhancement in real-time," *IEEE Transactions on Pattern Analysis and Machine Intelligence*, 2020. **1, 2, 3, 4**
- [14] T. Wang, Y. Li, J. Peng, Y. Ma, X. Wang, F. Song, and Y. Yan, "Real-time image enhancer via learnable spatial-aware 3d lookup tables," in *Proceedings of the IEEE/CVF International Conference on Computer Vision*, 2021, pp. 2471–2480. **1, 2**
- [15] C. Liu, H. Yang, J. Fu, and X. Qian, "4D LUT: Learnable context-aware 4d lookup table for image enhancement," *arXiv preprint arXiv:2209.01749*, 2022. **1, 2, 3, 4**
- [16] Y. Jo and S. J. Kim, "Practical single-image super-resolution using look-up table," in *Proceedings of the IEEE/CVF Conference on Computer Vision and Pattern Recognition*, 2021, pp. 691–700. **1, 2, 3, 4, 5, 7, 8, 9, 10, 12**
- [17] C. Ma, J. Zhang, J. Zhou, and J. Lu, "Learning series-parallel lookup tables for efficient image super-resolution," in *European Conference on Computer Vision*. Springer, 2022, pp. 305–321. **1, 2, 3, 4, 7, 8, 9, 12**
- [18] J. Li, C. Chen, Z. Cheng, and Z. Xiong, "MuLUT: Cooperating multiple look-up tables for efficient image super-resolution," in *European Conference on Computer Vision*. Springer, 2022, pp. 238–256. **1**
- [19] F. Zhang, H. Zeng, T. Zhang, and L. Zhang, "CLUT-Net: Learning adaptively compressed representations of 3DLUTs for lightweight image enhancement," in *Proceedings of the 30th ACM International Conference on Multimedia*, 2022, pp. 6493–6501. **1**
- [20] C. Nvidia, "Cuda toolkit documentation," 2018. **1, 5**
- [21] Z. Wang, B. He, W. Zhang, and S. Jiang, "A performance analysis framework for optimizing OpenCL applications on FPGAs," in *2016 IEEE International Symposium on High Performance Computer Architecture (HPCA)*. IEEE, 2016, pp. 114–125. **1, 5**
- [22] F. Khorasani, R. Gupta, and L. N. Bhuyan, "Efficient warp execution in presence of divergence with collaborative context collection," in *Proceedings of the 48th International Symposium on Microarchitecture*, 2015, pp. 204–215. **1, 5**
- [23] R. Yang, R. Timofte, M. Zheng, Q. Xing, M. Qiao, M. Xu, L. Jiang, H. Liu, Y. Chen, Y. Ben *et al.*, "NTIRE 2022 challenge on super-resolution and quality enhancement of compressed video: Dataset, methods and results," in *Proceedings of the IEEE/CVF Conference on Computer Vision and Pattern Recognition*, 2022, pp. 1221–1238. **2, 5, 6, 8**
- [24] H. Yeo, C. J. Chong, Y. Jung, J. Ye, and D. Han, "Nemo: enabling neural-enhanced video streaming on commodity mobile devices," in *Proceedings of the 26th Annual International Conference on Mobile Computing and Networking*, 2020, pp. 1–14. **2**
- [25] P. Chen, W. Yang, L. Sun, and S. Wang, "When bitstream prior meets deep prior: Compressed video super-resolution with learning from decoding," in *Proceedings of the 28th ACM International Conference on Multimedia*, 2020, pp. 1000–1008. **2**
- [26] Z. Wang, A. C. Bovik, H. R. Sheikh, and E. P. Simoncelli, "Image quality assessment: from error visibility to structural similarity," *IEEE transactions on image processing*, vol. 13, no. 4, pp. 600–612, 2004. **2, 6**
- [27] G. J. Sullivan, J.-R. Ohm, W.-J. Han, and T. Wiegand, "Overview of the high efficiency video coding (HEVC) standard," *IEEE Transactions on circuits and systems for video technology*, vol. 22, no. 12, pp. 1649–1668, 2012. **2**
- [28] K. C. Chan, X. Wang, K. Yu, C. Dong, and C. C. Loy, "Understanding deformable alignment in video super-resolution," in *Proceedings of the AAAI conference on artificial intelligence*, vol. 35, no. 2, 2021, pp. 973–981. **2**
- [29] —, "Basicvsr: The search for essential components in video super-resolution and beyond," in *Proceedings of the IEEE/CVF Conference on Computer Vision and Pattern Recognition*, 2021, pp. 4947–4956. **2**
- [30] C. Yang, M. Jin, X. Jia, Y. Xu, and Y. Chen, "AdaInt: Learning adaptive intervals for 3d lookup tables on real-time image enhancement," in *Proceedings of the IEEE/CVF Conference on Computer Vision and Pattern Recognition*, 2022, pp. 17522–17531. **2**
- [31] R. A. Jacobs, M. I. Jordan, S. J. Nowlan, and G. E. Hinton, "Adaptive mixtures of local experts," *Neural computation*, vol. 3, no. 1, pp. 79–87, 1991. **3**
- [32] N. Shazeer, A. Mirhoseini, K. Maziarz, A. Davis, Q. Le, G. Hinton, and J. Dean, "Outrageously large neural networks: The sparsely-gated mixture-of-experts layer," *arXiv preprint arXiv:1701.06538*, 2017. **3**
- [33] M. Emad, M. Peemen, and H. Corporaal, "MoESR: Blind super-resolution using kernel-aware mixture of experts," in *Proceedings of the IEEE/CVF Winter Conference on Applications of Computer Vision*, 2022, pp. 3408–3417. **3**
- [34] D. Ulyanov, A. Vedaldi, and V. Lempitsky, "Instance normalization: The missing ingredient for fast stylization," *arXiv preprint arXiv:1607.08022*, 2016. **3**

- [35] A. L. Maas, A. Y. Hannun, A. Y. Ng *et al.*, “Rectifier nonlinearities improve neural network acoustic models,” in *ICML*, vol. 30, no. 1. Atlanta, Georgia, USA, 2013, p. 3. 3, 5
- [36] J. M. Kasson, S. I. Nin, W. Plouffe, and J. L. Hafner, “Performing color space conversions with three-dimensional linear interpolation,” *Journal of Electronic Imaging*, vol. 4, no. 3, pp. 226–250, 1995. 4
- [37] T. Xue, B. Chen, J. Wu, D. Wei, and W. T. Freeman, “Video enhancement with task-oriented flow,” *International Journal of Computer Vision*, vol. 127, no. 8, pp. 1106–1125, 2019. 5
- [38] X. Yang, W. Xiang, H. Zeng, and L. Zhang, “Real-world video super-resolution: A benchmark dataset and a decomposition based learning scheme,” in *Proceedings of the IEEE/CVF International Conference on Computer Vision*, 2021, pp. 4781–4790. 5
- [39] T. Wiegand, G. J. Sullivan, G. Bjontegaard, and A. Luthra, “Overview of the H. 264/AVC video coding standard,” *IEEE Transactions on circuits and systems for video technology*, vol. 13, no. 7, pp. 560–576, 2003. 6
- [40] H. Zhao, X. Kong, J. He, Y. Qiao, and C. Dong, “Efficient image super-resolution using pixel attention,” in *European Conference on Computer Vision*. Springer, 2020, pp. 56–72. 7, 8
- [41] J. Cao, Y. Li, K. Zhang, and L. Van Gool, “Video super-resolution transformer,” *arXiv preprint arXiv:2106.06847*, 2021. 8
- [42] X. Wang, K. C. Chan, K. Yu, C. Dong, and C. Change Loy, “Edvr: Video restoration with enhanced deformable convolutional networks,” in *Proceedings of the IEEE/CVF Conference on Computer Vision and Pattern Recognition Workshops*, 2019, pp. 0–0. 8

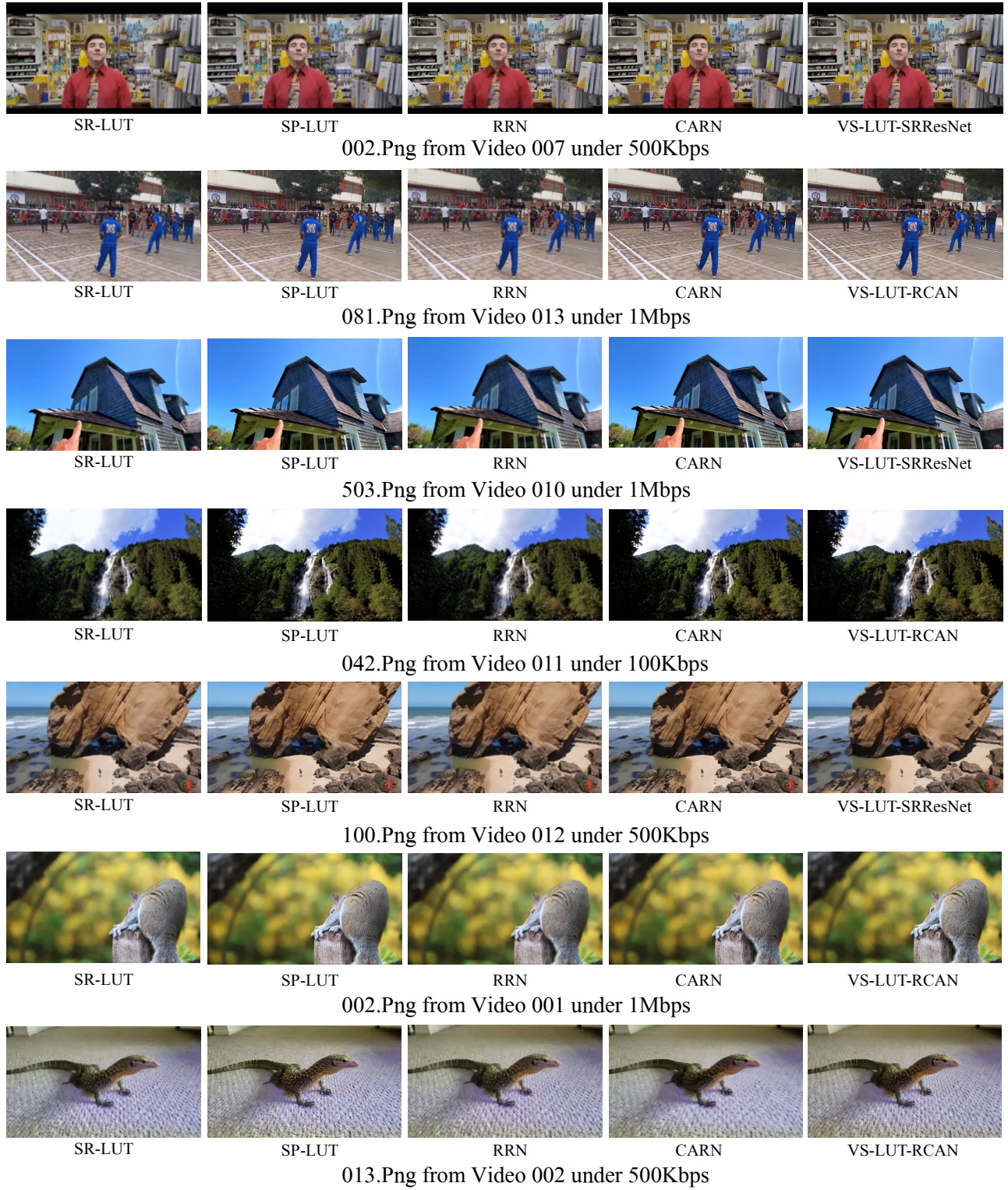


Fig. 6. More qualitative comparisons of SR-LUT [16], SP-LUT [17], RRN [2], and CARN [5] on our LDV-WebRTC testset.